Materials Technology Reports 2026, 4(1), 4049.
doi: https://doi.org/10.59400/mtr4049

Article

Effect of Si addition on the phase formation of Ni_2Al_3 and NiAl in plasma paste aluminizing of IN-738 superalloy

Ahmad Reza Rastkar*, **Taha Shariati**

Laser and Plasma Research Institute, Shahid Beheshti University, Tehran 1983969411, Iran

*** Corresponding author:** Ahmad Reza Rastkar, a-rastkar@sbu.ac.ir

CITATION

Rastkar AR, Shariati T. Effect of Si addition on the phase formation of Ni_2Al_3 and NiAl in plasma paste aluminizing of IN-738 superalloy. Materials Technology Reports. 2026; 4(1): 4049. https://doi.org/10.59400/mtr4049

ARTICLE INFO

Received: 24 February 2026
Revised: 1 June 2026
Accepted: 4 June 2026
Available online: 17 June 2026

Abstract: Ni superalloys are mostly used in turbine engines. But they suffer from high temperature oxidation. So, many investigations have been tried to protect the surface of these materials by pack aluminizing. A plasma paste process was used to aluminize the surface of superalloy IN-738. Nickel aluminum phases were created on the surface of the nickel-based superalloy IN-738 by plasma paste aluminizing with pure aluminum and Al-Si mixtures. Specimens were plasma-paste aluminized at 750–900 ºC for 1 h in low pressures of 10 mbar argon gas without Si and with 5–10% Si. Microstructural and compositional evaluations were studied using optical and scanning electron microscopes, EDS, X-ray diffraction (XRD) techniques, and Vickers microhardness tests. A mixture of fine or coarse equiaxed-grained microstructure of NiAl, Ni_2Al_3 with precipitates of Al_4Cr phases were observed in the coating layers. The addition of silicon showed the transformation of the NiAl and Ni_2Al_3 phases in the compound layers from fine-grained structures to nearly coarse equiaxed grains. In this plasma paste process, the silicon can be dissolved in the coating up to 10 at.% of the total coating composition and is mostly concentrated in some phases. Average Vickers microhardness analysis across the transverse cross section of aluminized samples under 500 g force revealed mostly an increase in hardness from approximately 250–300 HV0.5 in the substrate to 550–600 HV0.5 in the coating layers.

Keywords: IN-738 superalloy; plasma aluminizing; diffusion coatings; NiAl; Ni_2Al_3

1. Introduction

To increase the lifetime and performance of the blades and components operating at high temperature in advanced gas-turbine engines in high-temperature environments requires high resistance in high-temperature operations. Nickel-based superalloys are notable for high strength at high temperatures, significant resistance to oxidation and corrosion, high creep strength, heat resistance, excellent processability, and remarkable weldability [1]. To achieve this goal, it has required to exploit the significant performance of turbine blades made from nickel-based superalloys for increasing gas inlet temperatures and high temperature oxidation or corrosion resistance by surface transformation of these rotating materials. Diffusional aluminide coatings are largely applied on Ni-base superalloys to improve the high temperature corrosion resistance of these materials in high temperature corrosive environments [2,3]. Various methods can be used to produce different types of protective coatings, such as PVD (physical vapor deposition), CVD (chemical vapor deposition), PEPVD (plasma enhanced physical vapor deposition), PECVD (plasma enhanced chemical vapor deposition), or

diffusion coating processes, such as pack cementation and slurry methods. The coating microstructure and mechanical properties of these aluminide coatings depend on the parameters of different processes such as slurry aluminizing, pack cementation, and vapor deposition (CVD) [2,3].

In the diffusion process, it is essentially tried to create NiAl on Ni-based superalloy by diffusion of Al, in a single thermal treatment or in combination with the aluminizing process step [4]. The aluminizing process is basically carried out using a paste or pack cementation or process of chemical vapor deposition (CVD). The formation of the NiAl layer happens mostly by the decomposition of the previously formed layer of Ni_2Al_3 and the next inter-diffusion of Ni and Al. The nucleation and growth mechanisms of intermetallic phases of the Al-Ni system during pack aluminizing are based on the activity of aluminum in the pack. Ni_2Al_3 coating forms by inward diffusion of aluminum in a pack of pure aluminum with high activity [5]. Ni-rich NiAl coatings form by outward diffusion of nickel in a pack of Al-Ni alloy with low activity. The inward diffusion of Al first produces the intermetallic phase of Ni_2Al_3 which forms below the temperature of 1000 °C and high activity of Al. But, when the activity of Al in the pack or slurry is low and the process is carried out at a temperature higher than 1100 °C, Ni diffuses out and forms NiAl [6].

The aluminide coatings that contain a mixture of phases such as Ni_2Al_3, Al-rich NiAl, Ni-rich NiAl, and Ni_3Al form at high temperatures above 950 °C and with an outer layer of $NiAl_3$ grains. Deposition of electroless nickel before slurry aluminizing on René N5 Nickel-based superalloy at 700–1080 °C has enhanced the transformation of δ-Ni_2Al_3 to the β-NiAl phase [7]. This has happened near the Al-rich NiAl phase, which allows the inward diffusion of Al and outward diffusion of Ni [8]. Ni_3Al is an important phase in the Al-Ni system that may appear in the aluminizing of superalloys. In Ni superalloys, the coherent γ_0 phase with ordered $L1_2$ structure strengthens the γ matrix of superalloys. The ordered structure of the γ_0 phase depends on the exact location of Al and Ni atoms in the crystal lattice, which affects its behavior during high-temperature applications and deformation. The rigid phase of Ni_3Al obstruct the movement of dislocations from the γ matrix to provide the required strength for operation conditions [9]. Pack aluminizing on IN 600 superalloy has been carried out in a mixture of aluminum powder, NH_4Cl as an activator, and Al_2O_3 as a filler material at 650 to 700 °C. This aluminizing process has resulted in the formation of an inner layer of Ni_2Al_3 and an outer layer of Ni_3Al on the surface of the samples for oxidation protection [10].

Pack and vapor phase aluminizing processes are implemented with mixtures of aluminum powder, Al_2O_3 and a chemical activator at temperatures of 700 to 1050 °C. These kinds of diffusion aluminizing processes last for up to 20 h. These types of powder processes are divided into low, moderate, and high activated pack processes. At a high temperature of about 1050 °C, aluminide coatings such as NiAl phases are deposited with low activity, while NiAl phases with high activity that contain more aluminum form at about 700 °C [11]. The forming layer of nickel aluminide acts as a source of aluminum, which allows the film of alumina to form at high temperature to protect the substrate from oxidation by retarding oxygen diffusion. The process of

covering the surface with paste slurries yields the formation of nickel aluminide on the surface of IN-738 followed by subsequent heat treatment [12]. Vapor phase aluminizing of IN-792 with 24–30 wt.% Al content and 4–5 wt.% NH4Cl has showed a high-activity mechanism of inward diffusion of Al, which resulted in a three-layer coating with an outer layer of β-NiAl rich in Al [13]. At lower concentrations of Al and NH_4Cl, β-NiAl rich in Ni was created due to the dominance of the low-activity mechanism and outward diffusion of Nickel [14]. Alloying elements have had a great effect on the formation of NiAl aluminide coatings as an outer layer on IN-718 superalloy in CVD processes. By decreasing the concentration gradient of Al in the outer layer, the alloying elements have diffused out, and the inward diffusion of Al has dominated the growth of the coating at low temperatures with high activity, which has formed Ni_2Al_3 in the outer layer. At high temperatures with low activity, the rapid diffusion of Ni outwardly has formed Ni-rich β-NiAl as the main phase in coatings [15].

Modification of aluminide coatings with Zr on the nickel-base superalloy IN-738LC has been carried out by sputtering of Zr on the superalloy and subsequent heat treatment before pack aluminizing [16]. The high activity out-of-pack aluminizing resulted in an outer layer of NiAl and an intermediate layer with dissolved zirconium that showed high scale adhesion and low oxidation rates. While the addition of yttrium into the aluminide coatings of IN-738 by pack cementation process at 1000 °C had very poor resistance in comparison with the uncoated sample or the IN-738 sample which was aluminized directly [17]. Oxidation of a pack aluminized Ni-based superalloy IN-738L has resulted in an interdiffusion zone and the formation of α-Al_2O_3 scale at 1120 °C, while the coating at a lower temperature of 845 °C showed a different interdiffusion zone and γ-Al_2O_3 scale after oxidation at 1000 °C. During the heating in the oxidation process, two layers of NiAl, an outer layer and an interdiffusion zone, have formed via outward diffusion of Ni, which reacted with Al. While in high activity of aluminum, the two outer layers of NiAl and an interdiffusion zone have formed in addition to the precipitates enriched with Cr [18]. Initial coating of Cr before slurry coating on gas turbine parts has been used to protect the surface of the material. The barrier Cr layer has reduced the diffusion of aluminum into the substrate at 700 °C. However, annealing at 1200 °C the nickel atoms diffused outward from the substrate and in combination with Al from Al-Cr compounds formed NiAl compound which rejected the Cr element [19]. In this study, several Cr-rich and Si-rich phases were identified. The phases were composed of layers of Ni_3Al, NiAl, Al-rich NiAl, and Ni_2Al_3 [20].

Silicon has a great influence on the oxidation resistance of superalloys. It has been indicated that the addition of Si to chrome-containing aluminide coatings regulates the speed of Al diffusion in the coating, which optimizes the content of Al and increases the adhesion of the coating. This in turn increases the resistance to oxidation and the lifetime of the coating [21]. Silicon modified coating layers reduce the growth rate of oxides and increase the resistance of the superalloys during the long-time exposure to temperatures up to 1000 °C [22]. In fact, protective layers of Al-rich phases of NiAl intermetallic are typically formed in the coatings and change the mechanism of corrosion of the substrate. Addition of silicon in slurry aluminizing of IN-625

superalloys has controlled the thickness of the coating and uniformity precisely. The silicon addition has improved the oxidation and corrosion of the superalloys at high temperatures. Also, the solubility of chromium in the β-NiAl is low, but increases with increasing the amount of Ni to 28–30 at.% in the β-NiAl phase and leads to the formation of Cr deposits near or close to the β-NiAl phase [23]. Si-modified NiAl coatings with up to 9.0 at.% Si exhibited good oxidation resistance, better adhesion of Al_2O_3 layers, reduction of oxidation rate, and long protection in air at temperatures of 1100 °C [24] and 1000 °C [25]. Slurry aluminizing of IN625 superalloys with aqueous solutions of aluminum and silicon powders resulted in outer layers enriched with silicide compounds in the β-NiAl compound [26]. The average content of silicon has been from 5 to 15 wt.%. Pack cementation of IN-738 with the activator of NH4Cl and an inert filler of Al_2O_3 [27] has formed nickel silicides on the outer surface with a microhardness up to 1500 HV. Addition of cerium significantly increases the adherence of Al_2O_3 to the coating in the presence of silicon. When the content of cerium increases in the coating, it diffuses into the system and produces mismatches with β-NiAl, which reduces hot corrosion and oxidation resistance of the coatings due to spallation of the aluminide coatings [28].

Although the mechanism of formation of aluminide coatings in the techniques of the conventional pack cementation has been investigated and has been vastly controversial, there is not enough information in relation with the transformation mechanism of NiAl under the effect of Si in the plasma pack aluminizing methods. Plasma pack aluminizing is a very competitive procedure among different aluminizing techniques due to its low cost and versatility of applications [29]. AlSi aluminide coatings have been created by using plasma to irradiate aluminum and produce layers of NiAl and Ni_2Al_3 on the surface of K438G Ni superalloy [30]. The Si element has helped to a high level of oxidation resistance of the superalloy by increasing the activity of Al, which has enhanced the selective oxidation leading to α-Al_2O_3. Si has also formed silicide compounds of high-temperature elements such as W and Mo [30] for hot corrosion resistance and has hindered the interdiffusion of these refractory elements between coating layers. Si compounds have been coated on DD98M Nickel superalloy under plasma application. The coatings were produced quicker than that happens in diffusion-controlled thermal processes. The coatings are composed of aluminide compounds with dissolved Si or precipitates of silicides in the matrix of aluminide coatings. Higher power of radiation resulted in the formation of β-NiAl, while lower power created the δ-Ni_2Al_3 phase [31]. Heat treatment by oxygen plasma at 900 °C, 5 mbar pressures for 5 h after hot-dipping of Inconel 690 superalloy has created stable nanocrystalline Al_2O_3 on the top of the coating [32]. It is proposed that plasma application produces lattice defects in the surface of the material, which are followed by cascade collisions resulting in a mixture of defects. The cascade collision is also enhanced by the greater energy of ions in comparison with that of atoms in thermal treatments, which results in quick diffusion of elements [33].

As there are very limited in-depth studies devoted to the role of Si in the transformation of Ni_2Al_3 to NiAl under irradiation by plasma, it was worth investigating the effect of the process parameter of Si under plasma irradiation

to reveal the possible variations in the microstructure and phases of the aluminized coating layers, which can be considered as a novel study. In this article, it was observed that the addition of silicon to the coatings transforms parts of Ni_2Al_3 and other phases to Al-rich or Ni-rich NiAl phases with considerable dissolved Si or Cr, which could be useful for higher temperature oxidation resistance.

2. Materials and methods

The substrate material used in this research was a Ni-base superalloy IN-738 (chemical composition shown in **Table 1**). The samples were cut into cubic shape with the size of 5 × 10 × 10 mm. All samples were first polished using SiC paper from number of 120 to 1500 grade. The polished samples were rinsed in acetone and alcohol.

Table 1. The chemical composition of the substrate of the Ni-based superalloy IN-738 (wt%).

Co	Cr	Al	Ti	Mo	Nb	W	Ta	C	Zr	Fe	S	B	Ni
8.5	16	3.46	3.47	1.88	0.92	2.2	1.7	0.11	0.05	0.08	0.001	0.01	Bal.

Coating pastes were prepared from pure aluminum with a size of 10 mm or a mixture of Al and 5 or 10% Si powder with a size of 5 mm. Ethylene glycol was used as an addition material into the mixture of pure Al or Al and Si powders to make a soft paste mixture. The paste was adhered to the samples and placed in the vacuum chamber and heated under plasma argon gas at 150 °C for 1.5 h in order to vaporize and remove the ethylene glycol. After heating, the past became hard and adhered to the samples. Then the power was increased to achieve the aluminizing temperature of 750 to 900 °C and hold for 1 h. The irradiation of glow discharge of argon gas helps to heat the samples to gain the required temperature which held for 1 h under 10 mbar.

In plasma heating, the electrons and ions are excited under collision of plasma gas in the sheath region without changing the Gibbs free energy, which is necessary for the reaction. The enthalpy and entropy changes provide the necessary heat at a quicker rate to heat the samples. In fact, this kind of heating comes from ohmic and stochastic heating of ions and electrons from the inner of the atoms and molecules. Therefore, less power is necessary and faster heating rates occur in plasma processing of materials in comparison with conventional heating. In conventional heating, the materials are heated by external heating sources, and the heat is transferred by radiation, convection, and conduction, which require more energy and a longer time to be produced around the sample and deposited [34].

Aluminizing at 750 °C was carried out to evaluate the possibility of a plasma paste aluminizing process at this temperature, as most aluminizing studies had started their investigations at temperatures around 700 °C. As plasma paste aluminizing at this temperature did not result in a continuous even surface, it was chosen to try it at higher temperatures, and the samples that were treated at 900 °C were selected for reporting the effect of Si addition to the surface layers.

The coating setup that was used for this plasma paste aluminizing process has been described previously [35]. The setup consisted of a vacuum chamber, a pulsed

DC power supply, and a gas distribution system. The conditions parameters of the coatings are summarized in **Table 2**.

Table 2. The conditions of plasma paste aluminizing of IN-738 samples.

Sample	Coating composition	Plasma paste aluminizing temperature–time
IN-738PPA750	Aluminum	750 °C–1h
IN-738PPA900	Aluminum	900 °C–1h
IN-738PPASi5	Aluminum + 5% Si	900 °C–1h
IN-738PPASi10	Aluminum + 10% Si	900 °C–1h

An optical microscope and a scanning electron microscope (SEM) were used to investigate the surface and cross-sectional microstructure of the coated samples. For metallographic analyses, the specimens were sectioned across the layers and mounted. The cross sections were polished using SiC emery papers of grades 120 to 1500 and finally polished by diamond paste. Energy dispersive X-ray spectroscopy (EDX) was employed to study the amounts of elements in the coated layer. The maps of elemental analysis (EDS) were also examined to study the distribution of elements in the phases. Phase identification in the coatings was determined by an X-ray diffractometer (XRD) with a kα wavelength of a Cu target. Vickers microhardness measurements of the samples were performed under a 500 gf load for 10 s on distinct places of the surface layers, and their average value was recorded. However, one set of indentation impressions has been shown in the results.

3. Results and discussion

3.1. Microstructural observations of plasma-paste aluminized coatings on IN-738

Figure 1 shows the images of the IN-738PC750 sample, which was plasma-paste aluminized at 750 °C for 1 h. As shown in the optical micrograph, the sample had a fine and equiaxed grain structure near the substrate (**Figure 1a**) and transformed to a rather columnar structure near the surface of the coating. To investigate the possible phases in this morphology, it was examined with SEM microscopy (**Figure 1b**). The two regions of nearly equiaxed (region I) and columnar grains (region II) in **Figure 1b** can be observed in **Figure 1c**,**d** respectively. The grains of the region I (**Figure 1c**) and region II (**Figure 1c**) are mainly composed of NiAl phase (gray phase A), which is in agreement with the results from the EDX analyses (**Table 3**) in the columns of I-A and II-A. This phase was identified later in XRD analyses. The black phase B and light gray phase C (**Table 3, Figure 1c**,**d**) are strongly suggested to have a composition of a mixture of Ni_2Al_3 and Al_4Cr. This suggestion is more confirmed in the XRD patterns of the samples. From another point of view, the Al-Cr compounds appear with that of 20 to 30% Cr in the binary phase diagram of the Al-Cr alloy [20]. These compounds of Al and Cr have been reported in a wide range of aluminum and chromium contents [36]. Based on the experimental information, the following intermediate phases have been reported: Al_7Cr, $Al_{11}Cr_2$, Al_4Cr, Al_9Cr_4, Al_8Cr_5 and $AlCr_2$. As can be seen in the micrographs

of **Figure 1c**,**d** there are some very fine-grained phases in phase B that are Al-Cr phases dispersed in the Ni_2Al_3 phase (**Table 3**: I-B and II-B). Other investigations have reported the ternary phases of Ni-Al-Cr phases which form Ni_2Al_3 crystal structure and dissolve up to 20% chromium [20,37].

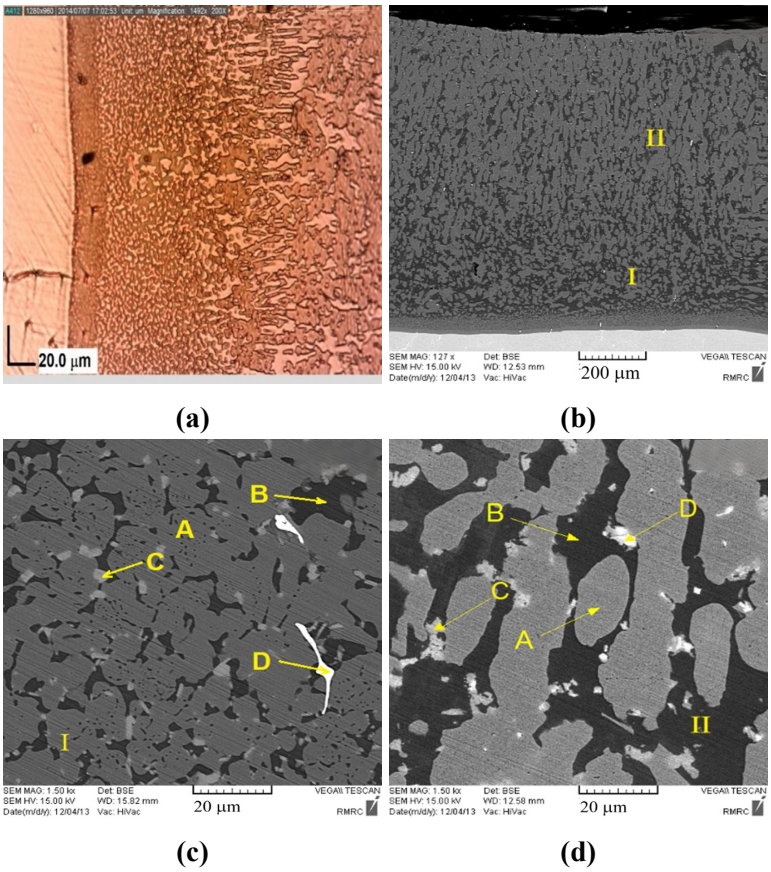

Figure 1. The images of plasma-paste aluminized coating on sample IN-738PPA750 at 750 °C for 1 h: **(a)** Optical micrograph; **(b)** SEM micrograph of two regions I and II, and the higher resolution of the microstructure showing the phases at points A, B, C, and D of regions **(c)** I; **(d)** II.

Table 3. EDX point analyses on IN-738PPA750.

EDX point analyses on IN-738PPA750	I-A (gray) at%	II-A (gray) at%	I-B (black) at%	II-B (black) at%	I-C (light gray) at%	II-C (light gray) at%	I-D (white) at%	II-D (white) at%
Al	43.0	46.0	63.01	65.5	60.04	63.2	3.59	18.7
Ti	2.0	2.98	0.465	0.71	1.9	1.8	15.94	10.5
Cr	2.3	2.5	17.7	16.1	4.8	3.5	7.22	5.7
Ni	43.2	43.2	11.4	12.1	7.15	6.2	7.11	12.8
Nb	3.6	2.34	2.64	0.45	15.8	12.3	45.02	37.8
Mo	1.0	0.76	0.4	0.3	9.24	7.2	10.14	15.5
Possible Phases	NiAl	NiAl	Cr-rich Ni_2Al_3 + Ni rich Al_4Car	Cr-rich Ni_2Al_3 + Ni rich Al_4Cr	Nb and Mo rich Ni_2Al_3	Nb and Mo rich Ni_2Al_3	Ni-Al-Ti-Cr-Mo-Nb	Ni-Al-Ti-Cr-Mo-Nb

For short aluminizing time, it has been observed that the aluminized layer is divided into two sub-layers: a rich layer of Ni_2Al_3 on the IN-738 matrix and a rich layer of Ni_2Al_3 at the top surface. In long aluminizing time, the coatings are formed from uniform layers of mainly Ni_2Al_3 which contain some precipitates of Ni_2Al_3 and $AlCr_2$ [19]. The control of the formation of the coated layers is first carried out by

the reaction of Ni_2Al_3 phase between semi-liquid aluminum and nickel. After the formation of theNi_2Al_3 layer, the diffusion of nickel atoms out of the Ni_2Al_3 layer controls the growth of Ni_2Al_3 layer into the semi-liquid aluminum [19, 20]. $AlCr_2$ islands precipitate at the interface between the coated layer and the substrate due to the low solubility of chromium in Ni_2Al_3 [12,18–20].

Therefore, it is strongly suggested that point B is composed of Cr-rich Ni_2Al_3 and Ni-rich Al_4Cr. The phases of Ni_2Al_3 and Al_4Cr were identified in the XRD results. However, the amount of Al_4Cr is much less than that of Ni_2Al_3 and NiAl phases. The light gray phase at point C in **Figure 1c**,**d** is mainly composed of Ni_2Al_3 with a considerable amount of dissolved Mo and Nb (**Table 3**: EDX I-C and II-C) [30], which is named the Nb and Mo-rich phase of Ni_2Al_3. A very small amount of a remarkable white phase (point D) was observed in most coatings, which must be a combination of refractory metals existing in the initial composition of the superalloy IN-738 with a composition of Ni-Al-Ti-Cr-Mo-Nb (**Table 3**: EDX I-D and II-D). This compound occurs due to the segregation of heavy refractory elements such as Mo and Nb at high temperatures [30,38]. These compounds have a very limited amount to appear in XRD patterns. This segregation has been observed in the fabrication of a wall component of a Ni–Ti–Cr–Mo–Nb alloy for polar research and space exploration by using the welding wires of TA1 and Inconel 625 that showed the granular precipitates of this alloy in different phases composed of Ni, Cr, and Ti [39].

Increasing the temperature to 900 °C formed a fine equiaxed grain structure in the coating layers of the sample IN-738PPA900 by plasma paste aluminizing process [27]. The optical micrograph in **Figure 2a** and the SEM micrograph in **Figure 2b** show a nearly more uniform fine equiaxed grain structure in the coating of the sample IN-738PPA900. Therefore, SEM and EDX analysis were performed at the middle of the coating layer.

The gray phase at point A in **Figure 2c** that refers to the major part of the coating showed a NiAl composition (**Table 4**). This is related to the higher temperature of phase formation in the Ni-Al system. NiAl forms in a wide range of temperatures and is the first phase that nucleates in aluminizing coatings [18,19]. This is also observed in the Ni-Al binary phase diagram that the stable NiAl phase forms at temperatures as high as 1600 °C and is stable up to room temperature, while Ni_2Al_3 is nucleated at temperatures below 1100 °C [20]. Therefore, the main phase throughout the sample IN-738PPA900 is attributed to NiAl.

It is seen that chromium has concentrated in the black phase B (**Figure 2c**, **Table 4**). However, the percentage of the phase B is much less than that of the phase A (**Figure 2c**), but small peaks of Al_4Cr were observed in the XRD pattern of the sample IN-738PPA900. It is strongly assigned to the dissolution of considerable amounts of Ni in this structure [18–20]. Therefore, it is suggested that the phase B (**Table 4**) is a mixture of Cr rich Ni_2Al_3 and Ni rich Al_4Cr. So, the phase B is formed first due to outward diffusion of Cr and Ni from the substrate material [19,20] during the plasma paste aluminizing. Due to the limited solubility of Cr atoms in the NiAl phase, most of the Cr atoms migrated to the interface of the NiAl phase with other phases and created Cr rich phases or dissolved in Ni_2Al_3 phase [40]. In superalloy 738, Cr has the highest

concentration after Ni. Therefore, during the coating, Cr diffuses out of the alloy and combines with aluminum to form Al_4Cr or Cr rich Ni_2Al_3 [18,19,41].

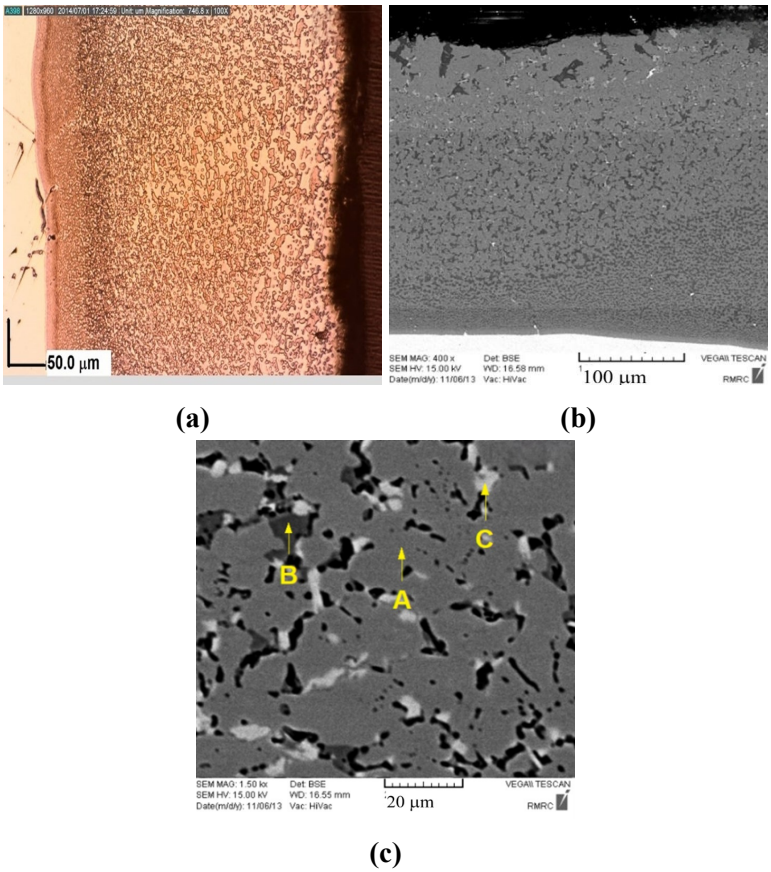

Figure 2. The images of plasma-paste aluminized coating on sample IN-738PPA900 at 900 °C for 1 h: **(a)** Optical micrograph; **(b)** SEM micrograph; **(c)** The higher resolution of the microstructure at the middle of the coating layer showing the phases at points A, B, and C.

Table 4. EDX point analyses on IN-738PPA900.

EDX point analyses on IN-738PPA900	Phase at point A (gray) at%	Phase at point B (black) at%	Phase at point C (light gray) at%
Al	45.8	66.5	60.04
Ti	2.0	0.465	2.2
Cr	2.3	16.7	4.8
Ni	42.2	11.4	7.15
Nb	3.6	2.64	14.8
Mo	1.0	0.38	9.24
Possible phases	NiAl	Cr rich Ni_2Al_3 + Ni rich Al4Cr	Nb and Mo rich Ni_2Al_3

As seen in **Figure 2c**, the main phase is NiAl (**Table 4**: phase A), Ni_2Al_3 (**Table 4**: phase B), and a few amounts of light gray phase of Ni_2Al_3 (**Table 4**: phase C) with considerable dissolved amounts of Mo and Nb. The phase C is labeled Nb and Mo rich Ni_2Al_3. This phase was not identified separately in the XRD pattern. Therefore, it is strongly assigned to a structure of dissolved Nb and Mo in Ni_2Al_3 [30]. It has been found that inward diffusion of Al is responsible for the formation of the Ni-rich NiAl phase, which is due to the decomposition of the Ni_2Al_3 phase at high temperature in diffusion processes. Therefore, the phase C formed due to outward diffusion of Ni from

the substrate material and inward diffusion of Al [18,19].

The addition of 5% silicon changes the microstructure in the sample IN-738PPASi5 (**Figure 3a**,**b**). The phase A (**Figure 3c**, **Table 5**) decreased in comparison with that in sample IN-738PPA900. In **Table 5**, it is seen that the Si element is concentrated in black phase B (**Table 5**). The low solubility of silicon in Ni_2Al_3proposes that the composition at point B resembles a combination of NiAl and Si rich Al_4Cr [4,30,31]. Again, a few amounts of light gray phase of Ni_2Al_3 (**Figure 3c**, **Table 5**: phase C) with considerable dissolved amounts of Mo and Nb is observed in sample IN-738PPASi5, which was labeled Nb and Mo rich Ni_2Al_3. Similar to sample IN-738PPA750, a very small amount of the remarkable white phase D (**Figure 3c**, **Table 5**) was observed in the coating with the same combination of refractory metals of Ni-Al-Ti-Cr-Mo-Nb in the coating of the superalloy IN-738.

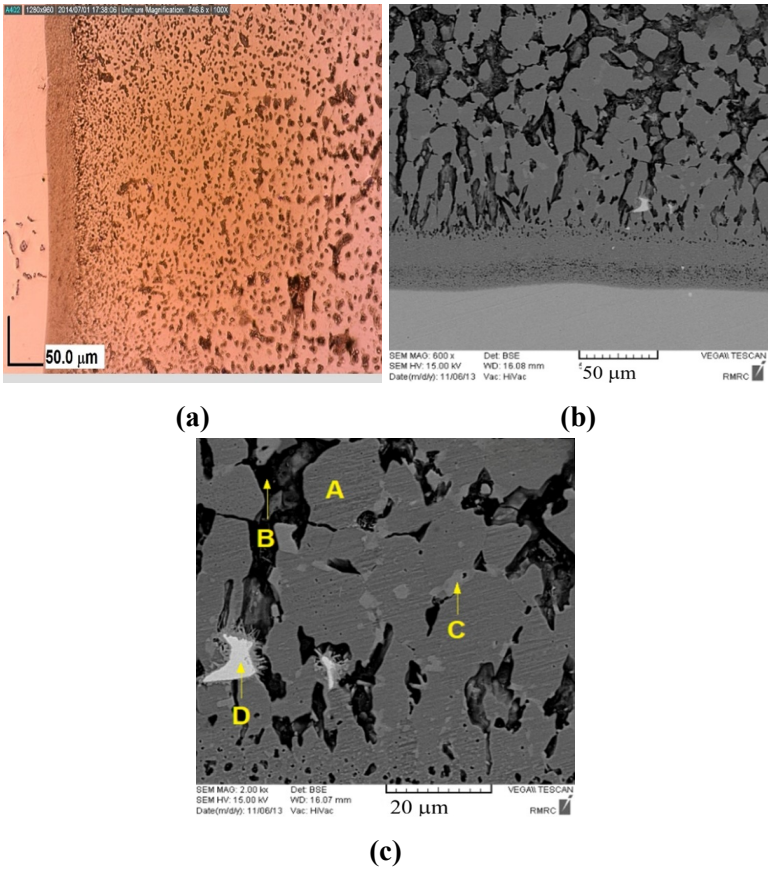

Figure 3. The images of plasma-paste aluminized coating on sample IN-738PPASi5 at 900 °C for 1 h with 5% Si: **(a)** Optical micrograph; **(b)** SEM micrograph; **(c)** The higher resolution of the microstructure showing the phases at points A, B, and C.

Table 5. EDX point analyses on the IN-738PPASi5 coating.

EDX point analyses on IN-738PPASi5 coating	Phase A (gray) at%	Phase B (black) at%	Phase C (light gray) at%	Phase D (white) at%
Al	65.97	31.93	69.13	3.79
Si	2.60	11.15	2.65	8.30
Ti	0.62	2.31	1.46	15.94
Cr	1.49	17.25	6.29	6.21
Ni	26.72	33.91	7.56	4.18
Nb	0.96	0.19	3.38	49.72

Table 5. *Cont.*

EDX point analyses on IN-738PPASi5 coating	Phase A (gray) at%	Phase B (black) at%	Phase C (light gray) at%	Phase D (white) at%
Mo	1.64	3.25	9.54	11.86
Possible Phases	Ni_2Al_3	NiAl + Si rich Al_4Cr	Nb and Mo rich Ni_2Al_3	Ni-Al-Ti-Cr-Mo-Nb

The EDS elemental map analysis (**Figure 4**) from the coating in **Figure 3** shows that the amount of Al has increased considerably from phase B to phases A and C, respectively. This is correlated to the outward diffusion of aluminum from NiAl in phase B and the formation of Ni_2Al_3 in phases A and C [18,19,29]. The EDS elemental maps of the sample IN-738PPASi5 (**Figure 4a**) are shown in **Figure 4b–h**. Al (**Figure 4b**) and Ni (**Figure 4c**) are mostly distributed in phases A and C (**Figure 3**), which can be attributed to the phase of Ni_2Al_3, as it was predicted before.

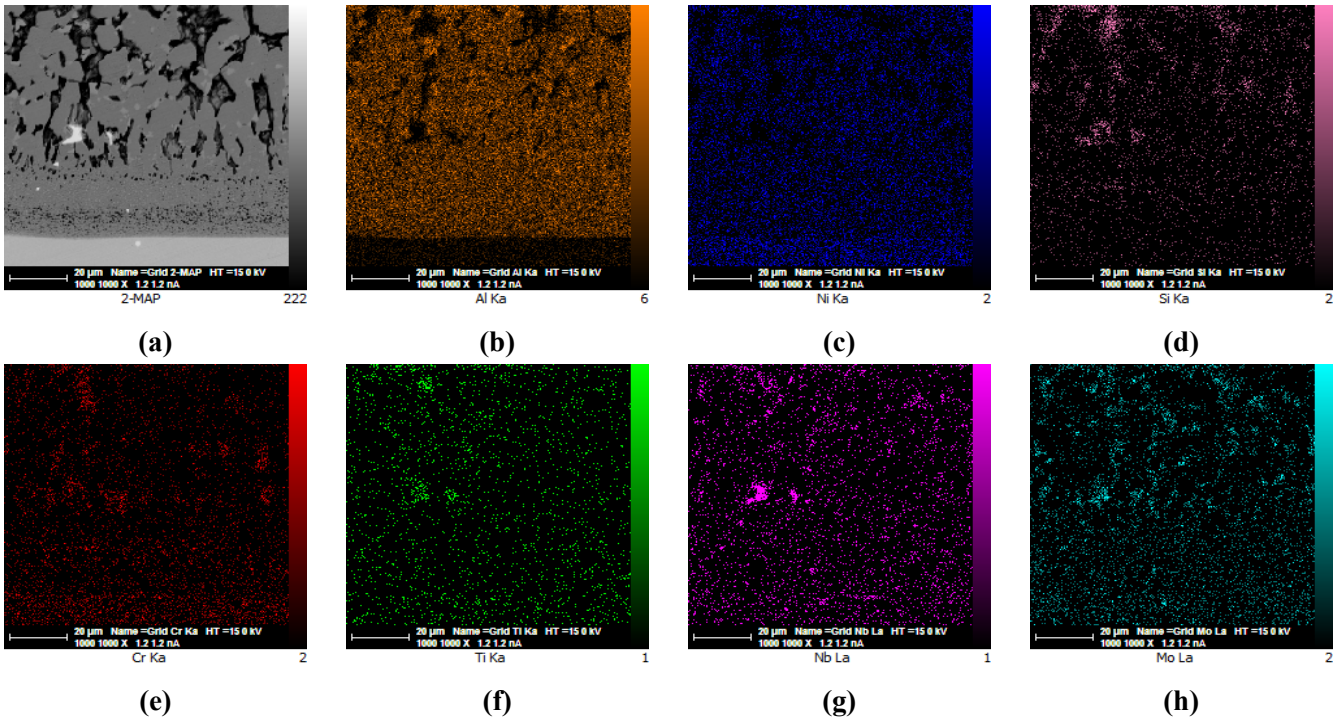

Figure 4. **(a)** SEM image and the corresponding EDS elemental maps of plasma paste aluminized coating on sample IN-738PPASi5 for: **(b)** Al; **(c)** Si; **(d)** Ti; **(e)** Cr; **(f)** Ni; **(g)** Nb; **(h)** Mo.

It is seen that Si (**Figure 4d**) and Cr (**Figure 4e**) have concentrated mostly in the black phase B (**Table 5**, **Figure 3c**), which can be related to the composition of Si rich Al_4Cr. However, the amount of Si with less than 3 at%, which has been distributed uniformly (**Figure 4d**) in the major phase of Ni_2Al_3 in phases A and C (**Table 5**, **Figure 3c),** is a characteristic of an aluminide coating that has been modified with Si during the application of the plasma paste aluminizing process. As Ti (**Figure 4f**), Nb (**Figure 4g),** and Mo (**Figure 4h**) are mainly distributed in phases C and D (**Table 5**, **Figure 3c**), they can be related to the compositions of Nb- and Mo rich Ni_2Al_3 in Phase C (**Table 5**, **Figure 3c**) and Ni-Al-Ti-Cr-Mo-Nb in phase D (**Table 5**, **Figure 3c)**. The very small amount of Ni-Al-Ti-Cr-Mo-Nb phase was also observed in sample IN-738PPA750, which can have the same origin as explained in that section.

As can be observed in samples IN-738PPA750, IN-738PPA900, and IN-738PPASi5, the microstructures are not layer by layer in comparison with those that occur in the coatings of most aluminizing processes. The coatings are composed of nearly equiaxed grains of NiAl and Ni_2Al_3 phases. These microstructures are related to the short-range inward diffusion of Al and outward diffusion of Ni in the adjacent powder particles with micrometer size, which cause the fast nucleation of Ni_2Al_3 phases and their conversion to NiAl phases [5–8,10,11,13–15] without enough time to grow in a long range to produce a continuous layer. The time of the plasma paste aluminizing process was much less than that of conventional [4–6] aluminizing processes. The fast nucleation is also the result of plasma ionization, excitation, and interaction of ions with neighboring atoms. It has been shown that plasma ions' interaction with a solid surface increases the rate of reactions among surrounding atoms and lowers the temperature and increases the enthalpy of the reaction [33, 34]. As it was observed in the experiments, no melting occurred during the processes, and the time of plasma paste aluminizing was rather less than that of other thermal diffusional aluminizing processes. However, the time of processes was low enough to prevent large grain growth of all phases.

Some preferential growth of NiAl phase happened in phase C (**Table 6**, **Figure 5c**) with the addition of 10% silicon to the coating powder mixture. The effect of the increase of Si up to 10% in the coating is observed in **Figure 5a**,**b**. It can be seen that the equiaxed grain structure of the sample IN-738PPASi5 has changed to a new equiaxed grain structure in which the phase C (**Table 6**, **Figure 5c**) has grown considerably in comparison with phase C in the sample of IN-738PPASi5, and the phase B (**Table 6**, **Figure 5c**) has reduced obviously in comparison with phase B in the sample of IN-738PPASi5. Cr, Nb, and Mo elements are soluble in Ni_2Al_3 structure and form Cr rich Ni_2Al_3 [18,19] in the phase A and Nb- and Mo rich Ni_2Al_3 in the phase D (**Table 6**, **Figure 5c**). The sum of the Cr, Nb, Mo, and Ni concentrations can be considered as the total Ni concentration in Cr rich Ni_2Al_3.

Table 6. EDX point analyses on the IN-738PPASi10 coating.

EDX point analyses on IN-738PPASi10 coating	**Phase A (gray) at%**	**Phase B (black) at%**	**Phase C (light gray) at%**	**Phase D (white) at%**
Al	76.54	45.90	38.13	61.63
Si	3.57	26.95	2.41	1.17
Ti	0.28	0.05	0.13	5.10
Cr	13.86	0.50	0.57	0.19
Ni	5.93	26.60	58.09	6.38
Nb	2.15	0.00	0.22	12.18
Mo	1.66	0.00	0.46	10.35
Possible Phases	Cr rich Ni_2Al_3	Si rich NiAl	NiAl	Nb and Mo rich Ni_2Al_3

It was observed that with increasing the Si content to 10% Si in the coating of the sample IN-738PPASi10, Ni_2Al_3 phase transformed to NiAl structure in phases B and C (**Figure 5c**). However, the amount of the phase B has reduced tremendously. The growth of phase C is the result of the diffusion of Si out of phase B (**Figure 5c**) due to exceeding the solubility of Si in phase B with Si rich NiAl composition [41]. As a result, the amount of phase B decreases and the phase C grows more, and this phase

forms with a high amount of Ni in the microstructure of sample IN-738PPASi10.

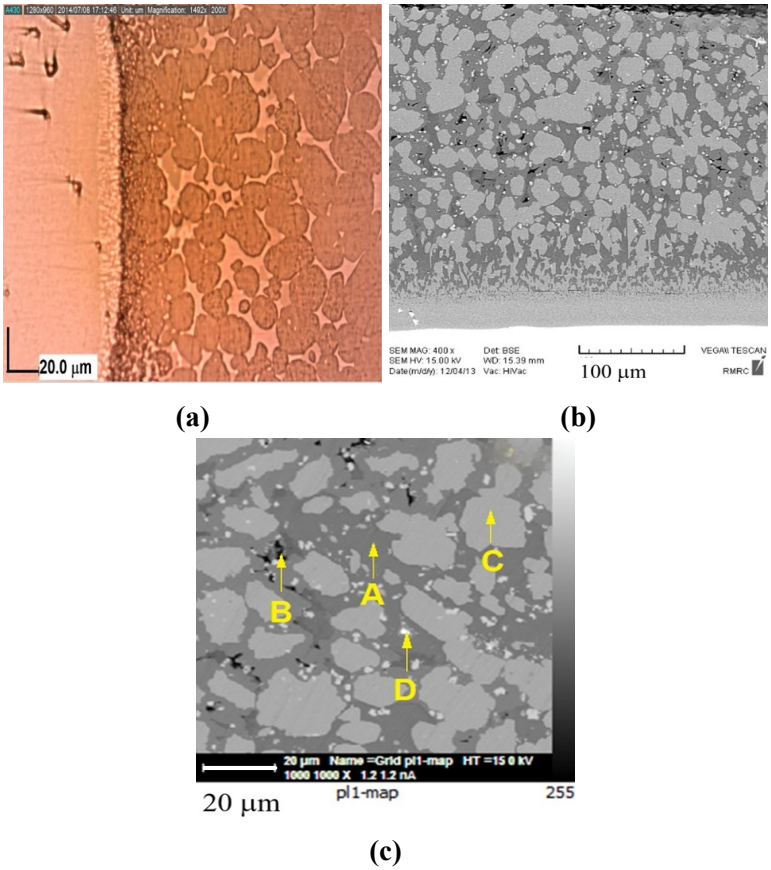

Figure 5. The images of plasma-paste aluminized coating on sample IN-738PPASi10 at 900 °C for 1 h with 10% Si: **(a)** Optical micrograph; **(b)** SEM micrograph; **(c)** Higher resolution showing points A, B, C, and D.

It has been observed that the Si content of the precipitated particles within the NiAl phase can contain up to 5 wt.% of the overall compositions of the particles [27,30,31,40]. However, there is an extra percentage of Si in phase B (**Figure 5c**, **Table 6**), which has been trapped in this phase, and the treatment time has not been enough to allow the Si to diffuse out of phase B. Some reports have also shown that the amount of Si which can be dissolved in NiAl is less than 0.4 wt.% [26,27]. Therefore, most of the Si content that is present in the NiAl phases is concentrated in the form of very small amounts of carbide particles or intermetallic phases that were not detected in XRD experiments. Diffusion of Ni in Ni_2Al_3 phase during heat treatment is negligible. But the diffusion of Al, which originates from the decomposition of the Ni_2Al_3, is more possible. Therefore, the inward diffusion of Al forms the Ni-rich NiAl phase C (**Figure 5c**, **Table 6**) at the interface of Ni_2Al_3 in phase A [5–8,10].

EDS elemental map analysis of the coating on sample IN-738PPASi10 (**Figure 6a**) confirmed most of the above postulations and suggestions. As it is seen in **Figure 6b**,**f**, the most amount of Ni has concentrated in phase C and has formed a Ni-rich phase of NiAl. This was predicted in the EDX results in **Table 6**. The chromium element has concentrated in phase A (**Figure 6e**) with a high amount of the aluminum element, which can be strongly attributed to the Ni_2Al_3 structure with a high concentration of dissolved chromium [18–20]. Therefore, the chromium-rich phase at point A is

assigned to the composition of Cr rich Ni_2Al_3. This is because of the lower diffusion of Cr in the NiAl phases that form during the coating process. The Si element (**Figure 6c**) is distributed mostly in phase B, then in phase A, and less in phases at points C and D. As a consequence, phase B with the least amount of Ni in NiAl structure is assigned to the composition of Si rich NiAl. From **Figure 6g**,**h**, the distribution of Nb and Mo can be related mostly to the precipitated islands of phase D (**Table 6**, **Figure 5c**). As phase D has a high concentration of aluminum, it can be related to a Ni_2Al_3 structure with the composition of Nb and Mo rich Ni_2Al_3.

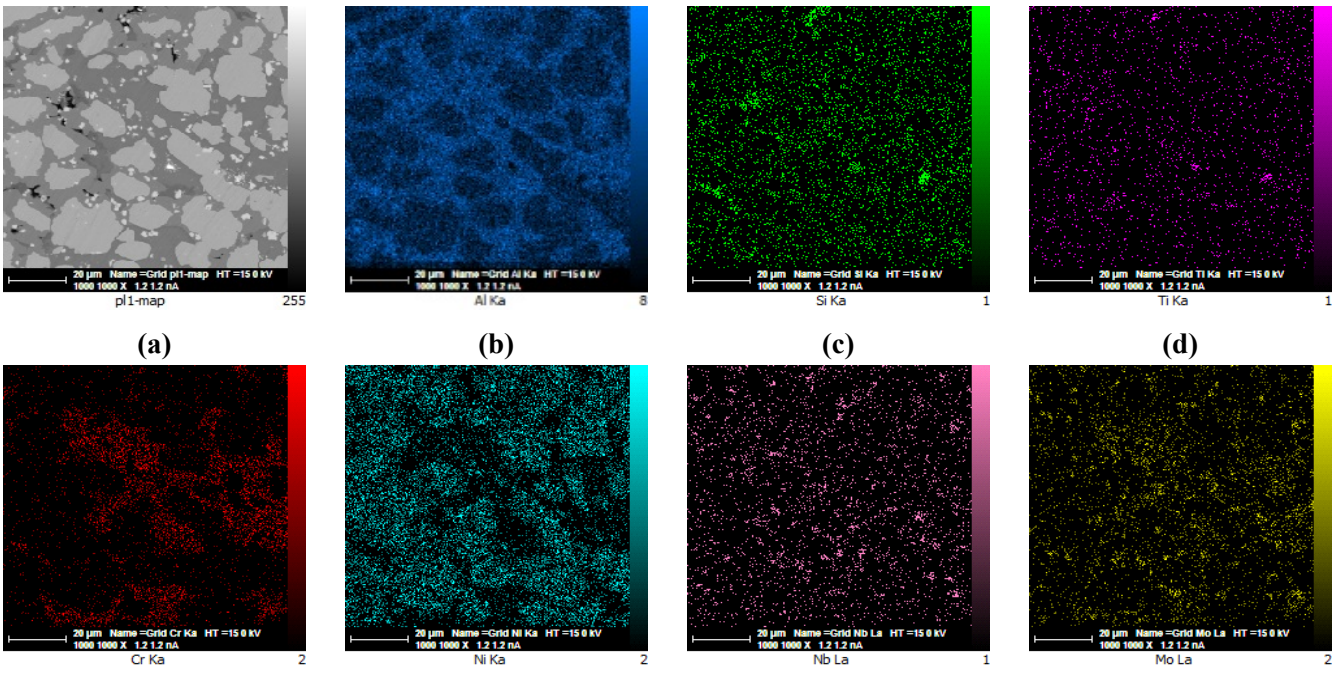

Figure 6. **(a)** SEM image and corresponding EDS elemental maps of plasma-paste aluminized coating on sample IN-738PPASi10 for: **(b)** Al; **(c)** Si; **(d)** Ti; **(e)** Cr; **(f)** Ni; **(g)** Nb; **(h)** Mo.

At temperatures at which aluminizing is carried out, nickel and other alloying elements present in IN-738 diffuse quickly into aluminum. So, the nickel concentration in aluminum increases very fast at the border between aluminum and the substrate of IN-738. As the solubility limit of nickel in semi-solid aluminum is reached, Ni_2Al_3 is formed. The diffusion of nickel atoms through the newly formed Ni_2Al_3 layer leads to the continuous formation of Ni_2Al_3 layer into the semi-solid aluminum. Therefore, the nickel concentration increases in aluminum and causes the growth of Ni_2Al_3 grains. As the aluminizing time increases, the first nucleated grains of Ni_2Al_3grow into the alloyed aluminum [41].

The growth of NiAl phase is due to the outward diffusion of Ni during the process that convert Ni_2Al_3 to NiAl [10, 11, 13–15]. It is believed that 10 at% Si in sample IN-738PPASi10 has helped the outward diffusion of Ni [13–15] which has been replaced with Si and resulted in the composition of Si rich NiAl in phase C (**Figure 5c**, **Table 6**) in the sample of IN-738PPASi10. If there has been any phase with the composition Al_4Cr in the sample IN-738PPASi10, it has been very low to be distinguished by XRD analysis (Subsection 3.2). It has been shown that, when NiAl

phase gets rich in Al, the outward diffusion rate of Ni decreases. This is due to the reaction of Ni with Al at the reaction border. Therefore, the grains of the coating grow by gradual outward diffusion of Ni into the Al-rich NiAl phase that initially forms in the coating. The new phase that forms in this transformation is less rich in Al, which in turn increases the outward diffusion of Ni, resulting in larger grains of the coating [10, 11, 13–15, 28]. This leads to a slightly lower Al concentration in phase C when compared to the grains A of the coating formed in phase A (**Figure 5c** and **Figure 6**). In Ni-rich NiAl, the diffusion coefficient of Ni is 3.5 times greater than that of Al. While in Al-rich NiAl, the diffusion coefficient of Al is about 10 times greater than that of Ni in Al-rich NiAl [13–15,28]. Therefore, the outward diffusion of Ni controls the interface between the zones of Ni-rich NiAl and Al-rich NiAl . In fact, the interface can only grow outward, towards the Ni-rich NiAl grains.

3.2. XRD patterns for phase identification of plasma-paste aluminized coatings on IN-738

As shown in **Figure 7**, the most possible phases that formed in the plasma-paste aluminized coating on IN-738 are Ni_2Al_3, NiAl and Al_4Cr. XRD analysis revealed diffraction peaks at crystallographic planes of (100), (101), (110), (102), (111), (200), (103), and (202) for Ni_2Al_3, diffraction peaks at crystallographic planes of (100), (031), (112), (110), (111), and (200) for NiAl and diffraction peaks at crystallographic planes of (100), (103), (101), (002), and (201) forAl_4Cr. It is observed in **Figure 7a** that Ni_2Al_3 is the most prominent phase in the coating of sample IN-738PPA750, with two distinctive peaks (110) and (102). Also, peaks of (100), (101), (111), and (202) have remarkable intensities in comparison with peaks of (110) and (102). These relative intensities are strongly correlated to the XRD pattern of Ni_2Al_3 [41].

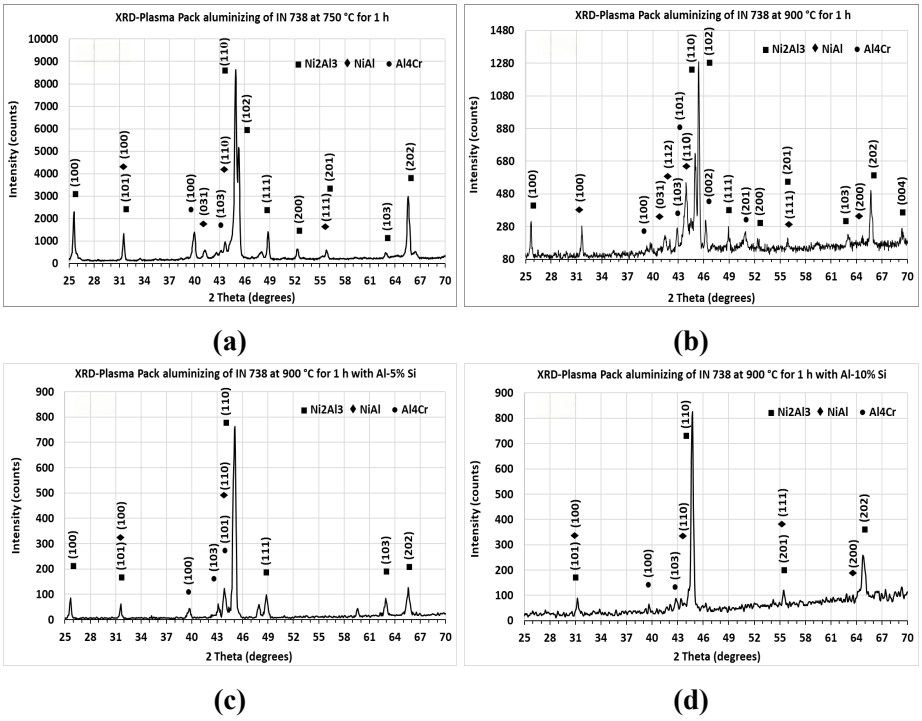

Figure 7. XRD patterns show the identified phases resulting from plasma paste aluminizing for samples **(a)** IN-738PPA750; **(b)** IN-738PPA900; **(c)** IN-738PPASi5; **(d)** IN-738PPASi10.

The strong peaks of (100), (101), (110), and (202) for Ni_2Al_3 are seen in the patterns of all samples. The observation of these peaks indicated strongly on the existence of Ni_2Al_3 in all samples. The variation in the intensity of some crystallographic planes is related to the variation of some dissolved elements of Cr, Nb, and Mo in Ni_2Al_3 structure. At 900 °C and with the addition of Si, the dominance of Ni_2Al_3 is slightly reduced, and NiAl phase grows in the phases of the samples, especially in samples IN-738PPASi5 and IN-738PPASi10, as seen in **Figure 7c**,**d**. However, in **Figure 7d**, the peaks of NiAl have reduced, but some peaks of Ni_2Al_3 have disappeared. This indicated the growth of NiAl phase in comparison with Ni_2Al_3, which agrees with the observations and EDX analysis of **Table 6** in **Figure 5** and EDS results in **Figure 6**.

3.3. Vickers microhardness measurements of plasma-paste aluminized coatings on IN-738

The integrity and adhesion between the coatings and the superalloy substrate are very important in such pack aluminizing processes. To study the coherency and matching of the mechanical properties of the coating and superalloy substrate, the region across the boundary between the substrate and coating was tested using micro-indentation tests.

Figure 8 shows the features of the microhardness indentations on the samples IN-738PPA750, IN-738PPA900, IN-738PPASi5, and IN-738PPASi10. As can be seen in **Figure 8**, however, there is a sharp boundary between the substrate and the aluminide coatings; no cracking, defects, or other mismatches were observed in the region between the coating and the substrate. Therefore, it is proposed that the plasma aluminizing process has not affected the microstructure and bulk properties of the Inconel substrate considerably. However, the hardness of the coating is significantly less than that of the Inconel substrate. The increase in the hardness of the coatings is strongly assigned to the nanocrystalline structure of the coatings rather than to the composition of the compounds in the coatings [42]. The microhardness of NiAl is about 600 HV, and that of Ni_2Al_3 is around 1100 HV [27]. The average microhardness of the region between the substrate and the coating is 590 HV0.5, which contains NiAl and Ni_2Al_3. The microhardness of the coating which contained more Ni_2Al_3 is 903 HV0.5, which is close to the hardness of Ni_2Al_3 [27]. The cross-sectional microstructures of plasma-paste aluminized IN-738 are shown in **Figure 8** at different conditions. It is seen that in all conditions, the coating layers have smaller indentation impressions than the substrate, which resemble a higher hardness in the coating than that of the substrate.

The average values of the microhardness of the substrate and coatings on IN-738 have shown in **Figure 9** at different conditions. These micro-indentation measurements were carried out at 3 to 5 rows across the cross section of the samples, and their average was recorded. However, the small variation in the value of hardness may be due to small errors in the measurements, it is worth discussing the relations between these variations and the phases formed in coatings. The majority of the coating in samples IN-738PPA750 (**Figure 1**) and IN-738PPA900 (**Figure 2**) consisted of phase A with the nominated composition of NiAl. This NiAl phase is surrounded by dispersed

phases of B and C with the overall composition of Ni_2Al_3. The microhardness of NiAl phase is around 600 HV, and that of Ni_2Al_3 Phase is about 1100 HV. Therefore, the average hardness of the coatings in samples IN-738PPA750 and IN-738PPA900 (**Figure 9**) is between 800 and 900 HV0.5. The lower hardness of the coating on sample IN-738PPA900 can be due to the formation of NiAl phase at the higher temperature of 900 °C.

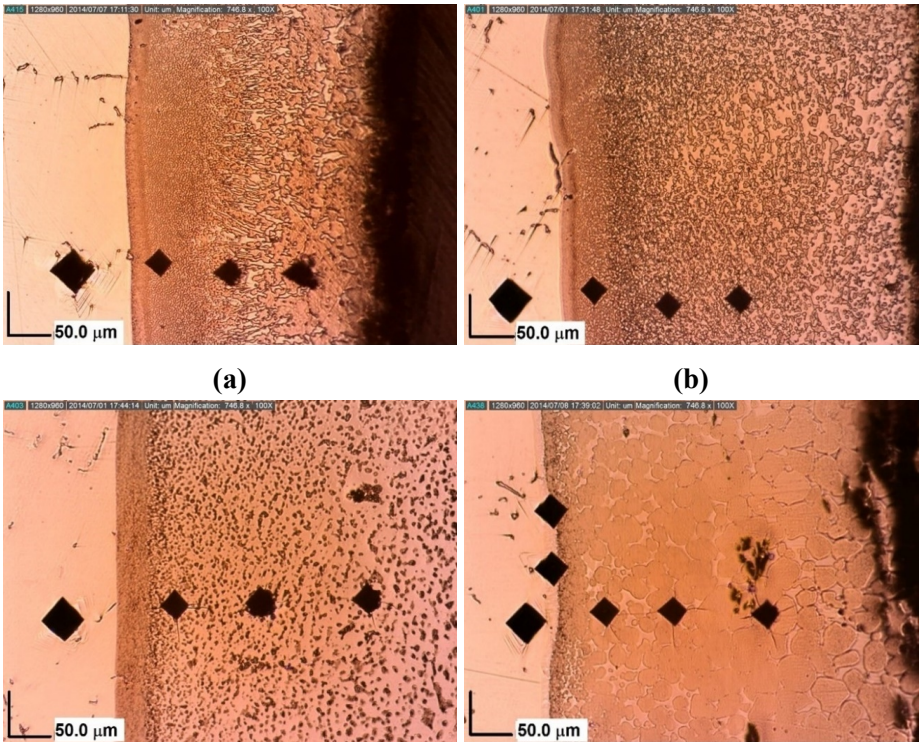

Figure 8. Optical micrographs show the indentation impressions of Vickers microhardness tests across the substrate and coating of plasma-paste aluminized samples of **(a)** IN-738PPA750; **(b)** IN-738PPA900; **(c)** IN-738PPASi5; **(d)** IN-738PPASi10.

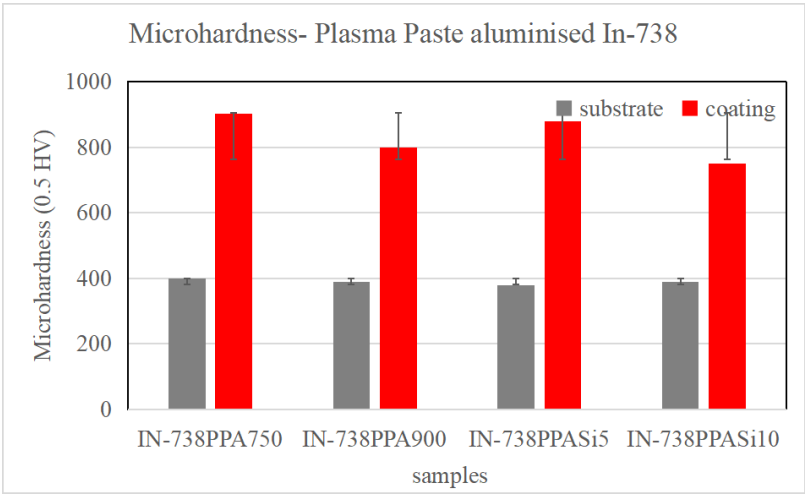

Figure 9. The variation of the microhardness values of the substrate and coatings on the IN-738 samples plasma-paste aluminized under different conditions, including the standard error bars.

Addition of 5% Si to the coating increases the hardness slightly in the sample of IN-738PPASi5. This increase is assigned to the contribution of more Ni_2Al_3

composition in phases A and C and the presence of Si rich Al_4Cr phase in combination with NiAl in phase B. Finally, the hardness in the sample IN-738PPASI10 is due to the growth of phase C (**Table 6**, **Figure 5c**) with a high amount of nickel in the composition of NiAl. In fact, the higher nickel has reduced the hardness of NiAl phase C (**Table 6**, **Figure 5c**) or is mainly composed of a softer NiAl phase. Also, the higher the amount of phase C had a greater contribution to the decrease in the hardness of the coating in this sample. Overall, despite these justifications, the variation in the hardness values of the coatings is not considerable, and it may also be originated from the error in the measurements that has been shown as error bars in **Figure 9**.

4. Conclusion

Plasma paste aluminizing of IN-738 resulted in coatings with a fine microstructure of mixed NiAl and Ni_2Al_3 phases rather than separate layers of these phases. Cr and Si were dissolved in NiAl and Ni_2Al_3phases, which are assigned as Cr rich Ni_2Al_3, Si rich NiAl. Some fine precipitates appeared among NiAl and Ni_2Al_3 phases with the assigned composition of Si rich Al_4Cr. Heavy metals such as Mo and Nb were found in the phase of Ni_2Al_3 with the assigned composition of Nb and Mo rich Ni_2Al_3. However, they were found as separate fine precipitates with a composition of Ni-Al-Ti-Cr-Mo-Nb. The amount of silicon and the temperature of plasma paste aluminizing had the main roles in the transformation of the phase structures. Silicon addition at a temperature as high as 900 ℃ showed the major influence on the phase structure of NiAl and Ni_2Al_3. Addition of 10% silicon enhanced the most variations in the grain structure of NiAl and Ni_2Al_3 phases in the plasma paste aluminizing of IN-738 from a fine structure to a round, equiaxed, and coarser grain structure. The Vickers microhardness of the coatings on IN-738 after plasma paste aluminizing was higher than that of the substrate. But there was not a great variation in the hardness of the coatings of different samples in comparison with each other. These negligible variations may be from measurement errors in addition to the changes in grain structure of the NiAl and Ni_2Al_3 phases.

Author contributions: Conceptualization, ARR; methodology, ARR; validation, ARR; formal analysis, ARR and TS; investigation, ARR and TS; resources, ARR; data curation, ARR and TS; writing—original draft preparation, ARR; writing—review and editing, ARR and TS; visualization, ARR and TS; supervision, ARR; project administration, ARR; funding acquisition, ARR. All authors have read and agreed to the published version of the manuscript.

Funding: This work received no external funding.

Institutional review board statement: Not applicable.

Informed consent statement: Not applicable.

Data availability statement: No new data were created.

Acknowledgement: The authors would like to acknowledge Shahid Beheshti University in Tehran, Iran, for the financial support of this study (using laboratory equipment in Shahid Beheshti University).

Conflict of interest: The authors declare no conflict of interest.

AI use statement: The authors declare that no artificial intelligence (AI) tools were used in the preparation of this manuscript.

References

1. Kopec M, Przygucka D, Mierzejewska I, et al. Effect of printing orientation on microstructure and fatigue behaviour of additively manufactured Haynes 282. Journal of Alloys and Compounds. 2025; 1036: 181777. doi: 10.1016/j.jallcom.2025.181777.
2. Piotrowska K, Kopec M. A Comprehensive Review on Aluminide Coatings for Ni-Based Superalloys: From Processing to Performance. Coatings. 2026; 16(4): 506. doi: 10.3390/coatings16040506
3. Kopec M. Recent Advances in the Deposition of Aluminide Coatings on Nickel-Based Superalloys: A Synthetic Review (2019–2023). Coatings. 2024; 14(5): 630. doi: 10.3390/coatings14050630
4. Arabi H, Rastegari S, Salehpour Z, et al. Formation mechanism of silicon modified aluminide coating on a Ni-base superalloy. IUST International Journal of Engineering Science. 2008; 19(5–1): 39–44. Available online: http://ijiepr.iust.ac.ir/article-1-124-fa.html
5. Thevand A, Poize S, Crousier JP, et al. Aluminization of nickel-formation of intermetallic phases and Ni_2Al_3 coatings. Journal of Materials Science. 1981; 16(9): 2467–2479. doi: 10.1007/BF01113583
6. Kalkan Y, Yener T, Yener SC, et al. Interface-Engineered Aluminide Coatings for Enhanced X-ray Shielding of Ni-Based Superalloys: Effect of Si and Co Additions. Arabian Journal for Science and Engineering. 2026; doi: 10.1007/s13369-026-11274-2
7. Kepa T, Bonnet G, Pedrizzetti G, et al. Slurry Aluminizing of Nickel Electroless Coated Nickel-Based Superalloy. Coatings. 2025; 15(11): 1337. doi: 10.3390/coatings15111337
8. Sarraf S, Rastegari S, Soltanieh M. Deposition of a low-activity type cobalt-modified aluminide coating by slurry aluminizing of a pre-Co-electroplated Ni-based superalloy (IN-738LC). Journal of Materials Research and Technology. 2024; 30: 1183–1193. doi: 10.1016/j.jmrt.2024.03.132
9. Rakoczy Ł, Milkovič O, Rutkowski B, et al. Characterization of γ′ Precipitates in Cast Ni-Based Superalloy and Their Behaviour at High-Homologous Temperatures Studied by TEM and in Situ XRD. Materials. 2020; 13(10): 2397. doi: 10.3390/ma13102397
10. Yener T, Doleker KM, Erdogan A, et al. Wear and oxidation performances of low temperature aluminized IN600. Surface and Coatings Technology. 2022; 436: 128295. doi: 10.1016/j.surfcoat.2022.128295
11. Hetmanczyk M, Swadzba L, Mendala B. Advanced materials and protective coatings in aero-engines application. Journal of Achievements in Materials and Manufacturing Engineering. 2007; 24(1). Available online: http://jamme.acmsse.h2.pl/papers_vol24_1/24148.pdf
12. Visuttipitukul P, Limvanutpong N, Wangyao P. Aluminizing of Nickel-Based Superalloys Grade IN-738 by Powder Liquid Coating. Materials Transactions. 2010; 51(5): 982–987. doi: 10.2320/matertrans.M2009382
13. Beni AA, Rastegari S. Microstructural investigation of low-activity and high-activity aluminide coatings fabricated by vapor phase aluminizing on IN792 superalloy. Scientific Reports. 2025; 15(1): 25284. doi: 10.1038/s41598-025-10549-2
14. Beni AA, Rastegari S. Mechanism reversion from outward to inward diffusion in gas-phase aluminizing: The effect of powder composition on coatings for IN792 superalloy. Vacuum. 2026; 252: 115491. doi: 10.1016/j.vacuum.2026.115491
15. Shao M, Mo W, Wu Y, et al. Research on the microstructure and diffusion behavior of CVD aluminide coatings on inconel 718 superalloy. Vacuum. 2024; 228: 113541. doi: 10.1016/j.vacuum.2024.113541
16. Latifi R, Rastegari S, Razavi SH. Effect of ZR Content on Oxide-Scale Spallation of Aluminide Coating. Iranian Journal of Materials Science & Engineering. 2019; 16(4). doi: 10.22068/ijmse.16.4.63
17. Tu DC, Lin CC, Liao SJ, et al. A study of yttrium-modified aluminide coatings on IN-738 alloy. Journal of Vacuum Science & Technology A: Vacuum, Surfaces, and Films. 1986; 4(6): 2601–2608. doi: 10.1116/1.573734
18. Sarraf S, Soltanieh M, Rastegari S. Isothermal oxidation performance at 1000 °C of two different aluminide coatings deposited by the reactive air aluminizing (RAA) method on a nickel-based superalloy (IN-738LC). Journal of Alloys and Compounds. 2025; 1010: 178123. doi: 10.1016/j.jallcom.2024.178123

19. Grégoire B, Bonnet G, Pedraza F. Development of a new slurry coating design for the surface protection of gas turbine components. Surface and Coatings Technology. 2019; 374: 521–530. doi: 10.1016/j.surfcoat.2019.06.020
20. Grégoire B, Montero X, Galetz MC, et al. Effect of chromium and silicon additions on the hot corrosion resistance of nickel aluminide coatings. Corrosion Science. 2023; 224: 111517. doi: 10.1016/j.corsci.2023.111517
21. Yener T, Erdogan A, Doleker KM, et al. Protective nickel silicide coating on Inconel 738 superalloy: Microstructure and wear behavior. Materials Today Communications. 2025; 43: 111643. doi: 10.1016/j.mtcomm.2025.111643
22. Ma, D, Fan Q, Wang T, et al. High temperature oxidation resistance and degradation mechanism of Al-Si coatings on a nickel-based superalloy at 1000 °C. Rare Metal Materials and Engineering. 2024; 53(2): 509–519. doi: 10.12442/j.issn.1002-185X.20230042 (in Chinese)
23. Miraboutalebi SV, Shirvani K, Kaflou A, et al. Microstructure and hot corrosion behavior of slurry silicon-aluminide coating modified by chromizing and chromium plating on superalloy Rene-80. Scientific Reports. 2025; 15(1): 43458. doi: 10.1038/s41598-025-27230-3
24. Zhang L, Zhou Y. Oxidation Behavior of Si-Modified Aluminide Coatings on K438 Superalloy Prepared Using a Hybrid Slurry/Pack Cementation Process. Corrosion. 2023; 79(1): 111–120. doi: 10.5006/4150
25. Dai Y, Zou J, Ning X, et al. Microstructure evolution and oxidation behavior of silicon-modified aluminide coatings on IN718 superalloy at 1000 °C. Journal of Central South University. 2024; 31(5): 1426–1442. doi: 10.1007/s11771-024-5653-0
26. Bakhtiary O, Sarraf S, Soltanieh M. Microstructure evaluation of Si-modified aluminide coatings on IN625 deposited by slurry aluminizing process. Surface and Coatings Technology. 2025; 495: 131592. doi: 10.1016/j.surfcoat.2024.131592
27. Yener T, Celebi Efe G, Keddam M, et al. Characterization and Growth Kinetics Modelling of Nickel Silicides Formed on Inconel 738 Alloy. Metals and Materials International. 2025; 31(11): 3190–3203. doi: 10.1007/s12540-025-01942-7
28. Nourpoor P, Javadian S, Aghdam ASR, et al. Microstructure Investigation and Cyclic Oxidation Resistance of Ce-Si-Modified Aluminide Coating Deposited by Pack Cementation on Inconel 738LC. Coatings. 2022; 12(10): 1491. doi: 10.3390/coatings12101491
29. Mahmoudi H, Hadavi SMM, Palizdar Y. Characterization, growth kinetics and formation mechanism of aluminide coating by plasma paste aluminizing on IN-738. Vacuum. 2021; 184: 109968. doi: 10.1016/j.vacuum.2020.109968
30. Wang W, Lei Y, Wu J, et al. Single-phase Si-modified β-NiAl coating formed by irradiation of Al-Si plasma: Microstructure and oxidation behavior. Corrosion Science. 2024; 233: 112055. doi: 10.1016/j.corsci.2024.112055
31. Wang W, Li Z, Lei Y, et al. Si modified aluminide coatings on a Ni-base superalloy prepared using Al-Si plasma irradiation: Growth mechanism and oxidation behavior. Surface and Coatings Technology. 2024; 494: 131425. doi: 10.1016/j.surfcoat.2024.131425
32. Zala AB, Samvatsar K, Desai V, et al. Plasma-Assisted Heat Treatments for Aluminide Coatings Deposition on Ni-Based Superalloys. Journal of Materials Engineering and Performance. 2025; 34(14): 14263–14271. doi: 10.1007/s11665-025-11027-6
33. Nastasi M. Mayer JW. Ion Implantation and Synthesis of Materials. Springer; 2010.
34. Lieberman MA, Lichtenberg AJ. Principles of Plasma Discharges and Materials Processing. John Wiley & Sons, Inc.; 2005.
35. Rastkar AR. Plasma enhanced paste aluminizing of Ti–45Al–2Nb–2Mn–1B with Al–Si alloys. Surface and Coatings Technology. 2015; 283: 10–21. doi: 10.1016/j.surfcoat.2015.10.036
36. Liang Y, Guo C, Li C, et al. Thermodynamic modeling of the Al–Cr system. Journal of Alloys and Compounds. 2008; 460(1–2): 314–319. doi: 10.1016/j.jallcom.2007.06.046
37. Audier M, Durand-Charre M, Laclau E, et al. Phase equilibria in the Al Cr system. Journal of Alloys and Compounds. 1995; 220(1–2): 225–230. doi: 10.1016/0925-8388(94)06010-X
38. Telbakiroğlu YB, Konca E. Effect of Aluminizing on the Oxidation of Inconel 718 and Inconel 738LC Superalloys at 925–1050 °C. Coatings. 2025; 15(12): 1482. doi: 10.3390/coatings15121482
39. Tian Y, Chen X, Cai Y, et al. Microstructure and properties of a Ni–Ti–Cr–Mo–Nb alloy fabricated in situ by dual-wire arc additive manufacturing. Materials Science and Engineering: A. 2022; 853: 143740. doi: 10.1016/j.msea.2022.143740
40. Romanowska J, Zagula-Yavorska M, Sieniawski J. Zirconium influence on microstructure of aluminide coatings deposited on nickel substrate by CVD method. Bulletin of Materials Science. 2013; 36(6): 1043–1048. doi: 10.1007/s12034-013-0579-4

41. Wu DL, Dahl KV, Grumsen FB, et al. Breakdown mechanism of γ-Al_2O_3 on Ni_2Al_3 coatings exposed in a biomass fired power plant. Corrosion Science. 2020; 170: 108583. doi: 10.1016/j.corsci.2020.108583
42. Parekh T, Patel P, Sasmal CS, et al. Effect of plasma processed Ti-Al coating on oxidation and tensile behavior of Ti6Al4V alloy. Surface and Coatings Technology. 2020; 394: 125704. doi: 10.1016/j.surfcoat.2020.125704